

Polymer melt dynamics and rotating frame nuclear spin relaxation

P. T. Callaghan

Department of Physics and Biophysics, Massey University, Palmerston North, New Zealand

(Received 7 December 1987; revised 23 June 1988; accepted 11 July 1988)

Nuclear spin relaxation time measurements may be used to probe the spectral density of polymer motion. It is shown that measurement of the rotating frame relaxation time, $T_{1\rho}$, extends the frequency range accessible to T_1 dispersions by over an order of magnitude. This frequency is sufficiently low to reveal tube renewal correlation loss in polyethylene melts and the $T_{1\rho}$ dispersions obtained here are well characterized by the tight tube model of Kimmich. In particular, a dependence of the spectral density on $f_1^{-1/2}$ is apparent where f_1 is the r.f. Larmor frequency. In addition to the tight tube subsystem, the entangled polymers also exhibit a region of spins where isotropic motion dominates and some cross-relaxation between these subsystems is observed. A feature of the tight tube relaxation dispersion is the molar mass independence of τ_1 , the correlation time for reptation around tube bends, thus suggesting that semi-local motion may be governed by fold length fluctuations.

(Keywords: melt dynamics; nuclear spin relaxation; polyethylene)

INTRODUCTION

Melt dynamics

Above a critical molecular mass, M_c , molten polymers are believed to form topological constraints known as entanglements. These entanglements govern the self-diffusion of the chains which are constrained to migrate along a curvilinear one-dimensional path in a 'tube' bounded by the topology of the surrounding polymer matrix¹⁻⁴. The classical determination of M_c is via the molar mass dependence of zero shear viscosity⁵. At M_c the viscosity exhibits a sudden change from approximately linear dependence on mass to a variation as $M^{3.4}$. M_c is typically of the order of 10^4 .

This paper is concerned with the microscopic nature of the molecular motion in the entangled regime and in particular with the use of the fluctuating dipolar interaction between nuclear spins as a probe of the spectral components of that motion. At the smallest distance scale the motion arises from segmental rotation about bonds. As a consequence of this rotation, defects arising from rotational isomers of neighbouring segments propagate and so a curvilinear one-dimensional diffusion of a labelled segment may be described, the so-called reptational motion⁶. Consider by contrast the largest distance scale of the centre of mass motion. In the de Gennes' model the polymer molecule is considered to move in a medium of semi-permanent constraints, and it may be shown that the time taken for complete disengagement from an initial tube (the reptation or tube renewal time) varies with molar mass as $\tau_R \sim M^3$. In consequence the polymer centre of mass self-diffusion over a macroscopic distance scale varies as $D \sim M^{-2}$.

In a later modification by Graessley⁷, the reptation model has been adjusted to allow for motion by the surrounding chains, an effect known as constraint release. Recent forward recoil scattering work⁸ on the centre of

mass self-diffusion of molten labelled chains in a matrix of variable molar mass has substantially verified the large scale motion predictions of the reptation model incorporating constraint release.

On the intermediate distance scale, smaller than the polymer dimensions but larger than the local segments, we are concerned with the translational motion of the polymer within the tube, the so-called 'semi-local' motion. It was shown by Doi and Edwards⁹ that this motion corresponds to a one-dimensional Brownian diffusion in which the centre of mass mean square displacement in three dimensions varies as $t^{1/2}$ rather than t , a consequence of confinement within the tube. The curvilinear diffusion coefficient D_1 depends simply on the total chain friction for one-dimensional motion and so $D_1 \sim M$.

The description in terms of curvilinear diffusion within a tube is somewhat simplistic. In addition to constraint release effects, the motion may be strongly influenced by the presence of chain folds unconstrained by entanglements⁷. Chain folds represent stored length and fluctuations in contour length associated with these folds not only enhance the tube disengagement but may also modify the semi-local motion.

Nuclear magnetic resonance relaxation time dispersions

Semi-local motion is difficult to observe experimentally since it corresponds to a distance scale between 100 Å and 1000 Å, too large for most neutron scattering experiments¹⁰ and too small for microdensitometry or pulsed gradient spin-echo n.m.r.¹¹ However it is possible, in principle, to observe both the semi-local and long range effects of reptation by monitoring the rotational correlations of polymer segments on a local scale. This facility depends on the existence of a residual correlation subsequent to local reorientation which remains to be

modulated by the longer range motion, an effect referred to as the 'tight tube' condition¹². The tight tube picture, applicable to polymer melts, has been the subject of a number of papers by Kimmich¹²⁻¹⁶ who has given a detailed description of the influence of the polymer dynamics on the spectral densities of fluctuating two spin dipolar interactions.

In order to probe these spectral densities, Kimmich and co-workers have used field cycling experiments¹⁷ in which the spin-lattice relaxation is measured under variable Zeeman polarizing fields. Using such a technique it is possible to employ Larmor frequencies as low as 10⁴ Hz during the relaxation process and still retain the sensitivity associated with observing the subsequent precession at several MHz. The present paper reports a modification of Kimmich's T_1 dispersion method which also retains the high field sensitivity but extends the lower frequency limit by over an order of magnitude. In this technique the nuclear spins relax in the rotating frame of the radiofrequency field which may be varied to probe the spectrum from 10² to 10⁵ Hz.

THEORY

Rotating frame relaxation

The spin temperature of an ensemble of nuclear spins in a magnetic field is determined by the ratio of the magnetization to the field amplitude. This spin temperature may therefore be decreased by isentropic demagnetization, an example of which is the 'spin-locking' experiment in which the large laboratory frame magnetization arising from the longitudinal polarizing field B_0 is reoriented along a much weaker orthogonal radiofrequency field B_1 so that the spin temperature is reduced by B_1/B_0 . In the presence of this resonant field the spin system relaxes to equilibrium with a time constant $T_{1\rho}$, the rotating frame relaxation time^{18,19}. In practice the condition for relaxation under spin-locked conditions is that the r.f. Larmor cyclic frequency, f_1 should exceed the zero field linewidth²⁰. The r.f. pulse and sampling sequence used for the measurement of $T_{1\rho}$ is given by $90|_x$ -(spin-lock duration t) $_y$ -acquisition.

The theory of nuclear spin relaxation has been extensively reviewed elsewhere²¹. Relaxation of the magnetization along a magnetic field requires energy exchange with the lattice reservoir and so relies on Hamiltonian terms fluctuating at frequencies corresponding to the relevant Zeeman splittings. For proton pairs (i, j) in polymeric methylene groups the predominant influence is the pair dipolar interaction \mathcal{H}_{ij} which comprises stationary rank 2 spin operators A_k modulated by a lattice fluctuations as given in equation (1).

$$\mathcal{H}_{ij} = \gamma^2 r_{ij}^{-3} \sum_k F_k A_k \quad (1)$$

The F_k are closely related to the spherical harmonic functions $Y_2^{(k)}(\theta_{ij}, \phi_{ij})$ where the θ_{ij} and ϕ_{ij} refer to the polar and azimuthal angles which the internuclear vector makes with the Zeeman field. The Fourier transforms of the autocorrelation functions of the three F_k components are the spectral densities, J_k . Under conditions for which BPP relaxation theory²² applies, it has been shown that

$T_{1\rho}$ is related to the J_k by

$$T_{1\rho}^{-1} = \frac{3}{2} \gamma^4 \hbar^2 I(I+1) \left[\frac{1}{4} J_0(2\omega_1) + \frac{5}{2} J_1(\omega_0) + \frac{1}{4} J_2(2\omega_0) \right] \quad (2)$$

where ω_1 and ω_0 are the Larmor frequencies for precession about the r.f. and longitudinal Zeeman fields, respectively (i.e. $\omega_1 = \gamma B_1$ and $\omega_0 = \gamma B_0$). The same theory applied to spin-spin (T_2) and spin-lattice (T_1) relaxation yields

$$T_2^{-1} = \frac{3}{2} \gamma^4 \hbar^2 I(I+1) \left[\frac{1}{4} J_0(0) + \frac{5}{2} J_1(\omega_0) + \frac{1}{4} J_2(2\omega_0) \right]$$

$$T_1^{-1} = \frac{3}{2} \gamma^4 \hbar^2 I(I+1) \left[J_1(\omega_0) + J_2(2\omega_0) \right] \quad (3)$$

It should be noted that while $T_{1\rho}^{-1} \rightarrow T_2^{-1}$ as $\omega_1 \rightarrow 0$ the result cannot be achieved in practice because ω_1 must always be sufficiently large to satisfy the Redfield condition²⁰. The spectral densities reduce to a particularly simple form for isotropic rotational diffusion²¹, namely,

$$J_0(2\omega) = b^{-6} (24/15) \tau_c / (1 + 4\omega^2 \tau_c^2)$$

$$J_1(\omega) = b^{-6} (4/15) \tau_c / (1 + \omega^2 \tau_c^2)$$

$$J_2(2\omega) = b^{-6} (16/15) \tau_c / (1 + 4\omega^2 \tau_c^2) \quad (4)$$

where τ_c is the rotational correlation time. Under extreme narrowing conditions, $\omega \ll \tau_c^{-1}$ and the high frequency J_1 and J_2 components of $T_{1\rho}^{-1}$ are given by $0.7 T_1^{-1}$. This relationship will prove useful in extracting the $J_0(2\omega_1)$ spectral density function from $T_{1\rho}$ measurements.

Kimmich three-step correlation model

In order to place the rotating frame relaxation method in context it is appropriate to briefly review the spectral density function associated with polymer reptation and derived by Kimmich^{15,16}. This model is aptly illustrated in Figure 1 of reference 16. For a chain confined to a tight tube formed by the matrix of neighbouring chains the anisotropic reorientation of the spin dipole-dipole interaction is the most rapid process and is designated component A . The correlation time for this motion, τ_s , corresponds to the rotation time for a segment and is sufficiently short to cause extreme narrowing where the reorientation is isotropic. The existence of residual anisotropy is essential for the observation of motion on a timescale many orders of magnitude longer than segment rotation. For example, component B is due to further reorientation by one-dimensional reptative displacements around tube bends. In the Kimmich model, the final correlation loss from such motion is extremely slow and indeed sufficient correlation remains on the much longer time scale needed to observe component C , the final definitive correlation loss by tube disengagement. The model accounts for tube renewal by both reptation and by the weaker path fluctuation effects associated with chain contours stored in folds.

Providing that the three components of motion are stochastically independent, the overall correlation function for segment reorientation is given by

$$G(t) = G_A(t) G_B(t) G_C(t) \quad (5)$$

where despite the hierarchy of the processes the correlations between them can be ignored because of the vastly different time scales on which they operate. The separate correlation functions are given by

$$\begin{aligned} G_A(t) &= a_1 \exp(-t/\tau_s) + a_2 \\ G_B(t) &= \exp(t/2\tau_i) \operatorname{erfc}(t/2\tau_i)^{1/2} \\ G_C(t) &= p_c \exp(-t/\tau_R^c) + p_r \exp(-t/\tau_R^r) \end{aligned} \quad (6)$$

where $a_2(a_2=1-a_1)$ describes the residual anisotropy following segment rotation. τ_i (given by $l^2/2D_1$) is the time for curvilinear diffusion around the correlation length, l , of the tight tube orientation and τ_R^r and τ_R^c are the tube renewal time constants for reptation and contour length fluctuation weighted by p_r and p_c , respectively. In the model the mean tube length per fold, Δ_0 , and the extended tube length, L_0 , determine the mean contour length fluctuation, $2x_r=(L_0\Delta_0)^{1/2}$ and the weighting $p_c=2x_r/L_0$. Note that the contour length fluctuation in this model influences the tube renewal correlation C but not the semi-local behaviour B for which the time constant τ_i is influenced by reptation alone. Such a picture predicts $\tau_i \sim M$.

Kimmich's description therefore contains six adjustable parameters, τ_s , τ_i , τ_R^r , τ_R^c , Δ_0/L_0 , and a_1/a_2 . Its usefulness lies in the prediction of specific frequency scales and crossovers. The exact expression for the spectral density arising from equation (5) is given in reference 16 but it is helpful to summarize the spectral regimes applicable to $J_0(2\omega_1)$ which provides the dominant influence on $T_{1\rho}$. These are

Low frequencies ($2\omega_1 \ll 1/\tau_R^r$) and long chains ($\Delta_0 \ll L_0$)

$$J_0(2\omega_1) \approx 2a_2(2\tau_i\tau_R^r)^{1/2} \quad (7)$$

Intermediate frequencies ($1/\tau_R^r \ll 2\omega_1 \ll 1/\tau_i$)

$$J_0(2\omega_1) \approx 2a_1\tau_s + 2a_2(2\omega_1)^{-1/2}\tau_i^{1/2} \quad (8)$$

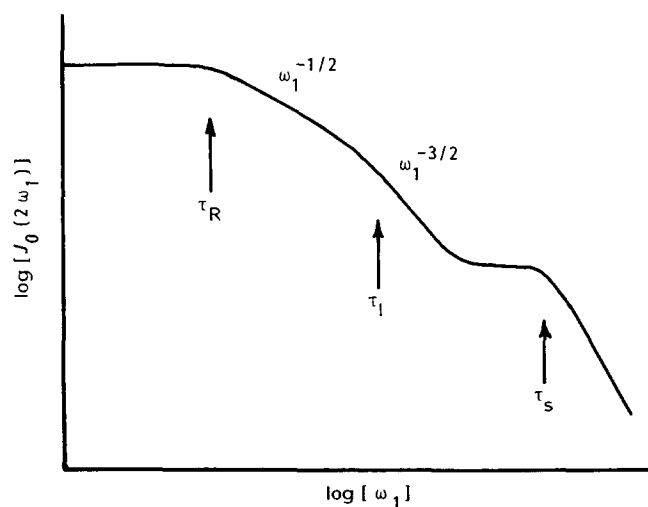


Figure 1 Schematic $J_0(2\omega_1)$ dispersion predicted by the tight tube reptation model of Kimmich. The frequency regimes defined in equations (7)–(9) are apparent along with their crossovers at frequencies τ_R^{-1} , τ_i^{-1} , τ_s^{-1} . The plateau between τ_i^{-1} and τ_s^{-1} arises from the predominant segmental motion and is the dominant influence on high frequency (MHz) T_1 relaxation

High frequencies ($2\omega_1 \gg 1/\tau_i$, $1/\tau_R^r$)

$$J_0(2\omega_1) \approx 2a_1\tau_s + a_2(2\omega_1)^{-3/2}\tau_i^{-1/2} \quad (9)$$

These regimes are depicted schematically in Figure 1.

In applying these spectral densities to the low frequency $T_{1\rho}$ dispersions it is important to establish that BPP relaxation theory is applicable. Suppose that the rigid lattice second moment is given by ω_p^2 . Then motional narrowing²¹ arising from a correlation time τ_c requires $(\omega_p^2\tau_c)^{1/2} \ll 1$. In the polymer example, the segmental reorientation leads to $(a_1\omega_p^2\tau_i)^{1/2} \ll 1$ but it is not clear that the anisotropic component, $a_2\omega_p^2$ is similarly narrowed. However it can be shown that motional narrowing yields a transverse relaxation rate of order $(a_2\omega_p^2\tau_c)$ which must be less than $1/\tau_c$ under BPP conditions. This provides a useful criterion. In the low frequency limit the effective polymer correlation time is $(\tau_R^r\tau_i)^{1/2}$ and the narrowing condition will break down for very long chains. The situation is however more favourable at the higher frequencies sampled by T_1 and $T_{1\rho}$ measurements. In the latter case it is apparent that BPP relaxation applies provided $\omega_1 \gg (a_2\omega_p^2)^{1/2}$ and hence spin-locking conditions are obeyed. It should be noted that in all the experiments performed here, the radiofrequency precession frequency exceeds the linewidth by over an order of magnitude except in the case of the 120 000 polymer where the smallest f_1 used is four times larger.

The problem of polymer spin–spin relaxation in the presence of a slowly fluctuating dipolar interaction has been investigated by Cohen-Addad^{23–25} whose description is based on Anderson–Weiss theory²⁶ and so yields a spectrum of relaxation times. While the polymeric motions incorporated in the Cohen-Addad and Kimmich descriptions differ somewhat, it is not the purpose of the present paper to distinguish between these two models which relate to spin–spin and spin–lattice relaxation, respectively. Although spin–spin relaxation measurements are presented here to demonstrate the validity of the tight tube assumptions, $T_{1\rho}$ measurements under spin-lock conditions yield BPP dispersions to which the Kimmich theory is specifically addressed.

Spin heterogeneity

It is well known that transverse relaxation in high molar mass polymer melts exhibits a distinct slowly relaxing component^{27,28} which decreases in relative amplitude with increasing molar mass. In the present work a slowly relaxing component is also visible in the rotating frame relaxation. One must be careful not to make a direct comparison between these slow components in T_2 and $T_{1\rho}$ because of the very different conditions which apply in the two types of measurement. Under spin-lock conditions where BPP relaxation theory applies, the relaxation of a given spin system should be single exponential. The existence of bi-exponential behaviour in present $T_{1\rho}$ experiments, at r.f. cyclic frequencies of up to 50 kHz, indicates the existence of spin heterogeneity.

The slow component relaxation time is only weakly dependent on molar mass and is comparable in magnitude with the single component rates observed in the spin relaxation of low molar mass ($M < M_c$) polymer melts. For these latter polymers entanglements do not exist and isotropic segment rotation occurs. It is therefore

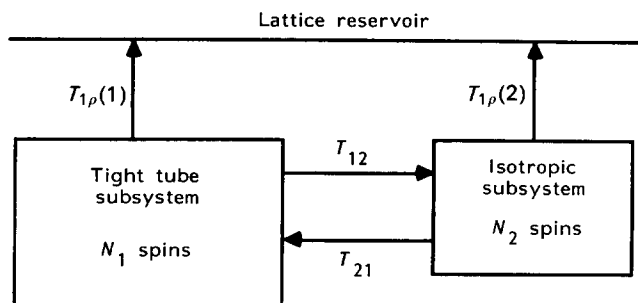


Figure 2 Coupled spin subsystem model used to interpret the bi-exponential rotating frame relaxation

Table 1 60 MHz proton spin-lattice and spin-spin relaxation times for polyethylene at 150°C. The spin-spin relaxation data for the higher molar masses are multi-exponential. Amplitudes of (possible) identifiable components are shown in brackets

Molar mass	2155	14 000	32 000	120 000
T_1 (s)	0.84 [1.00]	0.74 [1.00]	0.73 [1.00]	0.78 [1.00]
T_2 (s)	0.59 [1.00]	0.065 [0.74] 0.23 [0.26]	0.0090 [0.46] 0.036 [0.46] 0.14 [0.081]	0.0047 [0.68] 0.0175 [0.28] 0.11 [0.04]

reasonable to associate the high molar mass slow component with a physical region of the polymer where $a_2 = 0$ and extreme narrowing applies. Such heterogeneity in the melt may have a number of origins. It may arise from the presence of low molar mass components due to polydispersity. Alternatively isotropic rotation may occur on the ends of the chain where the polymer is undergoing continual tube disengagement or at regions within the chain where constraint release is taking place. Whatever its origin, heterogeneity will lead to multicomponent relaxation if spin-diffusion between the different physical regions is too slow to allow a common spin temperature to exist.

In the present work two distinct components are observed in $T_{1\rho}$ relaxation and so two spin subsystems are identified. To allow for the possibility of some cross-relaxation between these subsystems a coupled reservoir model²⁹ is employed as shown in Figure 2. Such a model predicts a bi-exponential decay with time constants τ_a , τ_b and amplitudes a , b dependent upon the number of spins in each reservoir, N_1 , N_2 , the respective rotating frame relaxation rates $T_{1\rho}^{-1}(1)$, $T_{1\rho}^{-1}(2)$ and the cross-relaxation rate T_{12}^{-1} . The relationships between these are given by

$$\tau_{a,b}^{-1} = \frac{1}{2} [A + C \pm [(A + C)^2 - 4(CA - DB)]^{1/2}]$$

$$a = N_1(A - B - \tau_b^{-1}) / (\tau_a^{-1} - \tau_b^{-1}) + N_2(A - \tau_a^{-1})(\tau_a^{-1} - \tau_b^{-1}) / [(A - \tau_a^{-1})(\tau_a^{-1} - \tau_b^{-1}) - (A - B - \tau_b^{-1})(A - \tau_b^{-1})]$$

$$b = 1 - a \quad (10)$$

where $A = T_{1\rho}^{-1}(1)^{-1} + T_{12}^{-1}$; $B = T_{12}^{-1}$

$$C = T_{1\rho}^{-1}(2)^{-1} + \left(\frac{N_1}{N_2}\right) T_{12}^{-1}; \quad D = (N_1/N_2) T_{12}^{-1}$$

EXPERIMENTAL

Monodisperse polyethylene was obtained from Polymer Laboratories (Church Stretton, Shropshire, UK) and included all available fractions above 2000, namely 2155 ($M_w/M_n = 1.14$), 14 000 ($M_w/M_n = 1.27$), 32 000 ($M_w/M_n = 1.10$), 120 000 ($M_w/M_n = 1.20$). The critical entanglement molar mass for polyethylene is 3800 (ref. 5) so that the polymers provide three examples above M_c and one below. Samples were placed in 4 mm diameter n.m.r. tubes, flushed with N_2 , pumped and sealed *in vacuo*. All experiments reported here were performed at 150°C using a Jeol FX60 n.m.r. spectrometer incorporating a specially built pulse programmer³⁰ and high power r.f. probe. All experimental parameters including the r.f. field amplitude were under software control. A Henry Radio 2006 A 600 W r.f. amplifier was used to provide spin lock fields up to $f_1 = 100$ kHz (where $f_1 = \omega_1/2\pi$). The apparatus was checked by measuring $T_{1\rho}$ for water at values of f_1 up to the maximum employed in the polymer experiments. Approximately 2 s was obtained in each case, consistent with $T_2 < T_{1\rho} < T_1$.

Spin-lattice and spin-spin relaxation

Table 1 shows the comparative T_1 relaxation obtained using the inversion-recovery method for the four polymer fractions. Single exponential behaviour with T_1 about 0.8 s is obtained in each case consistent with the dominant influence of the extreme narrowed isotropic (a_1) spectral density component at the high frequencies to which spin-lattice relaxation is sensitive. By contrast the T_2 relaxation is shown in Figure 3 in this case obtained using a Carr-Purcell-Meiboom-Gill sequence³¹. Here the relaxation is significantly molar mass dependent and multi-exponential behaviour is apparent for $M > M_c$. The data is summarized in Table 1. Both the T_1 and T_2 results reported here are consistent with earlier measurements by Koch *et al.*³² However in the case of T_2 , the data has been extended to greater times in order to more clearly reveal the slowly relaxing component. This 'extreme-narrowed subsystem' appears with an amplitude ranging from 0.04

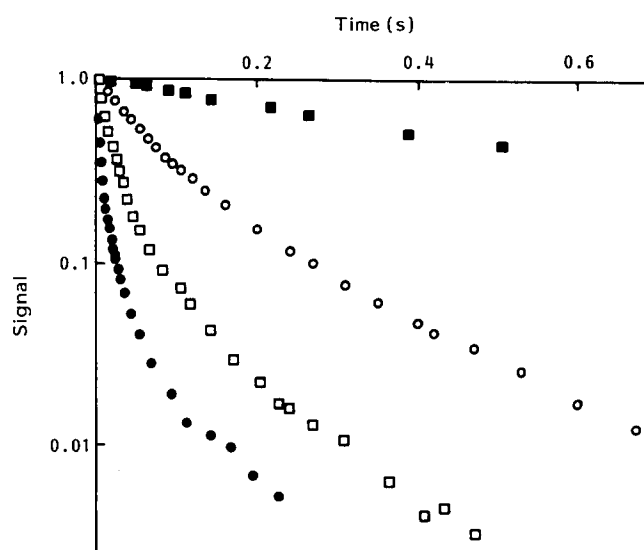


Figure 3 Transverse relaxation (logarithmic scale) for different molar mass for polyethylene melts at 150°C. The signal amplitude is plotted logarithmically. Data is obtained using a CPMG spin-echo pulse sequence. Molar mass fractions: ■, 2155; ○, 14 000; □, 32 000; ●, 120 000

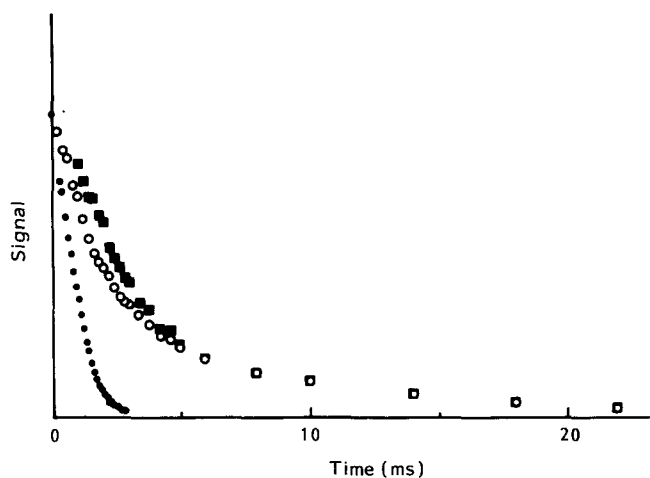


Figure 4 Transverse relaxation (linear scale) for 120 000 polyethylene melt using differing r.f. pulse sequences. The free induction decay following the single $90|_x^\circ$ r.f. pulse is subject to inhomogeneous broadening from rank 1 and rank 2 terms in the Hamiltonian. The $90|_x-180|_y$ and phase cycled $90|_x-90|_{x,y}$ sequences removed rank 1 and both rank 1 and rank 2 broadening, respectively. Note the identity of the data at long times where the signal is dominated by the isotropic subsystem. ■, $(90|_x, 90|_y)-(90|_x, 90|_x)$; ○, $(90|_x, 180|_y)$; ●, $(90|_x)$

in the case of fraction 120 000 to 1.00 in the case of fraction 2155. If this component is to be associated with spin heterogeneity and identified with a region of the polymer where conditions of tight tube anisotropy do not apply, then the long relaxation time magnitude should be influenced only by local segment rotation and therefore should not depend on molar mass. By contrast it is apparent from the gradual progression in the magnitudes of the slow relaxation times from lowest to highest molar mass that the more rapid anisotropic component is influential and so some cross-relaxation couples the differing spin subsystems.

All molar masses exhibit a degree of inhomogeneous (i.e. refocussable) broadening well in excess of that associated with magnet inhomogeneity. The effect is shown in Figure 4 for the 120 000 polyethylene melt where the free induction decay following a single 90° pulse is compared with the signal following a $90|_x-\tau-180|_y-\tau$ -echo sequence for which rank one spin tensors in the inhomogeneity Hamiltonian are refocussed. The spectral narrowing corresponds to a reduction in linewidth from 700 to 130 Hz in comparison with the magnet inhomogeneity of 20 Hz. Similar effects have been observed in experiments on polyethylene³² and polydimethyl siloxane²⁸ and have been associated, respectively, with internal magnetic anisotropy arising from holes in the melt and to residual static dipole-dipole interactions.

In fact these influences can be separated by an appropriate experiment since the $90|_x-\tau-180|_y$ sequence will not refocus the rank two dipolar interaction. What is needed, by comparison, is a pulse sequence capable of refocussing both rank one and rank two broadening. For this purpose, a phase cycled echo $90|_x-\tau-90|_{y,x}-\tau$ sequence was employed using weak homospoil field gradient pulses before and after the second r.f. pulse. It is straightforward to show that the difference signal is devoid of both rank one and rank two broadening. The results of such an experiment are also shown in Figure 4 where it is clear from the further lengthening of the decay,

in comparison with the $90|_x-\tau-180|_y$ experiment, that residual rank two spin operators are present in addition to the inhomogeneous broadening associated with internal magnetic anisotropy. By contrast a sample in which exclusively isotropic reorientation prevailed showed an identity between the two experiments. The extreme-narrowed subsystem responsible for the slow decay at long times in Figure 4 shows a similar identity.

The existence of static dipolar terms in the 120 000 polyethylene spin Hamiltonian points to the complexity of the transverse relaxation process in high polymer melts and the need to employ Anderson-Weiss theory in the zero frequency limit of the spectral density.

Rotating frame relaxation

Figure 5 shows the rotating frame relaxation for all four molar mass polyethylenes under an r.f. amplitude given by $f_1 = 1250$ Hz. The data for the fraction 2155 is single exponential with a relaxation time of 0.57 s, close to the T_2 limit. By contrast for $M > M_c$ multi-exponential behaviour is observed. Indeed the data appears bi-exponential and to test this hypothesis a double exponential least squares fit was applied yielding the values shown in Table 2. Such a fit is naturally more sensitive to the larger amplitude component. If each component is to be given equal weighting regardless of amplitude it is necessary to minimize residuals in the log domain. Such a fitting procedure is justified only if the signal-to-noise ratio of the data is high enough that the

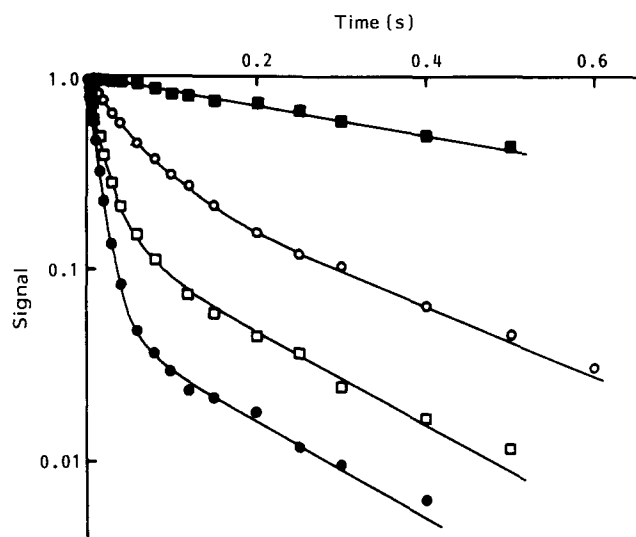


Figure 5 Rotating frame relaxation (logarithmic scale) for different molar mass polyethylene melts at 150°C . The apparently bi-exponential behaviour for $M > M_c$ is interpreted as resulting from the tight tube and isotropic spin reservoirs. The theoretical curves are least squares double exponential fits. Symbols as in Figure 3

Table 2 Decay time constants τ_a , τ_b and amplitudes a , b (in brackets) obtained by bi-exponential non-linear least squares fit to polyethylene melt rotating frame relaxation in the case $f_1 = 1250$ Hz

Molar mass	14 000	32 000	120 000
Linear domain			
τ_a	0.038 [0.56]	0.0140 [0.78]	0.0114 [0.93]
τ_b	0.19 [0.44]	0.12 [0.22]	0.12 [0.07]
Log domain			
τ_a	0.048 [0.67]	0.0163 [0.83]	0.0121 [0.94]
τ_b	0.24 [0.33]	0.17 [0.17]	0.16 [0.06]

The number of significant figures used specifies the precision of the measurement

Table 3 Proton rotating frame relaxation time constants and amplitudes for polyethylene melts at 150°C. The coupled spin model is used to obtain the rapid component $T_{1\rho}(1)$ values. The relative subsystem heat capacities, $N_1:N_2$ are obtained by fitting the lowest f_1 experiments

f_1 (Hz)	2155			$N_1 = 1.00$ $N_2 = 0$		14 000		$N_1 = 0.75$ $N_2 = 0.25$		32 000		$N_1 = 0.85$ $N_2 = 0.15$		120 000		$N_1 = 0.94$ $N_2 = 0.06$		
	τ_a	[a]	$(\tau_a = T_{1\rho}(1))$	τ_a	[a]	$T_{1\rho}(1)$	T_{12}	τ_a	[a]	$T_{1\rho}(1)$	T_{12}	τ_a	[a]	$T_{1\rho}(1)$	T_{12}	τ_a	[a]	
555	0.58	[1.00]		0.047	[0.66]	0.050	0.9	0.0137	[0.82]	0.0140	1.0	0.0070	[0.93]	0.0072	2.0			
				0.23	[0.34]			0.15	[0.18]			0.11	[0.07]					
833	0.58	[1.00]		0.050	[0.67]	0.052	1.0	0.0152	[0.83]	0.0155	1.2	0.0091	[0.93]	0.0092	2.5			
				0.24	[0.33]			0.16	[0.17]			0.13	[0.07]					
1250	0.57	[1.00]		0.048	[0.67]	0.051	1.0	0.0163	[0.83]	0.0163	1.2	0.0121	[0.94]	0.0122	3.0			
				0.24	[0.33]			0.17	[0.17]			0.16	[0.06]					
1670	0.55	[1.00]		0.049	[0.67]	0.052	1.0	0.0177	[0.84]	0.0180	1.2	0.0140	[0.95]	0.0141	3.5			
				0.25	[0.33]			0.18	[0.16]			0.18	[0.05]					
2500	0.55	[1.00]		0.050	[0.65]	0.053	1.2	0.021	[0.83]	0.0215	1.2	0.0184	[0.94]	0.0185	3.5			
				0.25	[0.35]			0.15	[0.17]			0.17	[0.06]					
4000	0.53	[1.00]		0.051	[0.68]	0.055	1.2	0.025	[0.84]	0.026	1.2	0.025	[0.95]	0.025	3.5			
				0.30	[0.32]			0.15	[0.16]			0.19	[0.05]					
6940	0.48	[1.00]		0.067	[0.77]	0.070	1.8	0.034	[0.82]	0.035	1.7	0.033	[0.93]	0.033	3.5			
				0.34	[0.23]			0.17	[0.18]			0.17	[0.07]					
10 000												0.040	[0.93]	0.041	4.5			
												0.21	[0.07]					
12 500	0.58	[1.00]		0.077	[0.77]	0.079	2.0	0.053	[0.88]	0.054	2.2	0.048	[0.95]	0.049	5.5			
				0.36	[0.23]			0.28	[0.12]			0.23	[0.05]					
16 670				0.075	[0.75]	0.078	2.0	0.064	[0.89]	0.065	3.0	0.058	[0.95]	0.059	6.0			
				0.36	[0.25]			0.30	[0.11]			0.27	[0.05]					
25 000	0.51	[1.00]		0.078	[0.79]	0.082	2.0	0.070	[0.90]	0.071	3.0	0.074	[0.94]	0.075	7.0			
				0.36	[0.21]			0.29	[0.10]			0.25	[0.06]					
35 710	0.52	[1.00]		0.078	[0.75]	0.082	2.0	0.085	[0.88]	0.085	3.5	0.092	[0.99]	0.092				
				0.33	[0.25]			0.30	[0.12]			0.87	[0.01]					
50 000	0.47	[1.00]										0.118	[1.00]	0.118				
62 500	0.47	[1.00]		0.11	[0.73]	0.120	2.0	0.100	[0.84]	0.100		0.122	[1.00]	0.122				
				0.32	[0.27]			0.29	[0.16]									
100 000	0.34	[1.00]		0.175	[1.00]	0.175		0.156	[1.00]	0.156		0.150	[1.00]	0.150				

Note that the cross-relaxation time T_{12} is only approximate

asymptotic behaviour of the slow component is clearly visible.

The results of the logarithmic fit are given in Table 2 and the corresponding curves are shown plotted against the data in Figure 5. The parameters obtained via the two fitting procedures are broadly similar although the slow component is noticeably better represented in the logarithmic fit. Not surprisingly the greatest discrepancy is found in the 14 000 fraction experiments for which the two exponentials had the most similar time constants and for which the asymptotic limiting behaviour was least apparent. The similarity of the linear and logarithmic fit parameters for the two higher molar masses lends some credence to the bi-exponential assumption although it is clear from the deviation from the fits apparent in Figure 5 that this assumption is only an approximation. The division of the spins into two coupled subsystems will lead to bi-exponential behaviour provided that each subsystem can be represented by a common spin temperature. The spin temperature assumption is of course implicit in previous use of T_1 dispersions to characterize the entire ensemble. In that sense the condition is relaxed in the present analysis by the further spin subdivision. The description used here cannot possibly be exact but it is a valid first approximation and it is justified to the extent that bi-exponential relaxation is observed.

The long $T_{1\rho}$ components decay at a rate comparable with the relaxation time in the 2155 ($M < M_c$) melt and, as with the T_2 data, there is a progression in rates as the $T_{1\rho}$ values of the rapid component lengthen with increasing molar mass. This provides further corroboration of the

coupled subsystem model in which the slowly relaxing component arises from segments undergoing rapid isotropic motional narrowing.

The data for all values of f_1 , summarized in Table 3, are represented by the three experimental parameters a/b , τ_a and τ_b , obtained by least squares fit in the logarithmic domain. In order to interpret the data using the model shown in Figure 2 and hence obtain the tight tube subsystem $T_{1\rho}(1)$ values, it is necessary to establish the parameters which characterize the subsystem. These are the relative heat capacities, N_1/N_2 , the cross relaxation rate, T_{12} , and the isotropic subsystem relaxation time, $T_{1\rho}(2)$. For this latter value the extreme narrowed T_1 limit of 0.8 s is assumed, an approximation justified by the dependence of T_1 on the 'segmental reorientation plateau' shown in Figure 1. The value of the slow component time constant, τ_b , is then determined to a large degree by cross-relaxation with the dominant spin subsystem, an effect which is clearly apparent in the data as previously indicated.

Figure 6 depicts the relationships between the various parameters. $T_{1\rho}(2)$ is held fixed while $T_{1\rho}(1)$ is varied. The effect of varying the cross-relaxation time is shown in Figure 6a, while 6b shows the influence of the heat capacity ratio. It is clear in Figure 6a that in the limit where $\tau_a \ll \tau_b$ the dominant influence of the cross-relaxation rate is on τ_b whereas τ_a is largely independent of T_{12} . Fortunately this is the regime in which most of the present experiments were performed so that the interpretation of the $T_{1\rho}(1)$ values is largely model independent. A similar independence of τ_a on N_1/N_2 is apparent in Figure 6b.

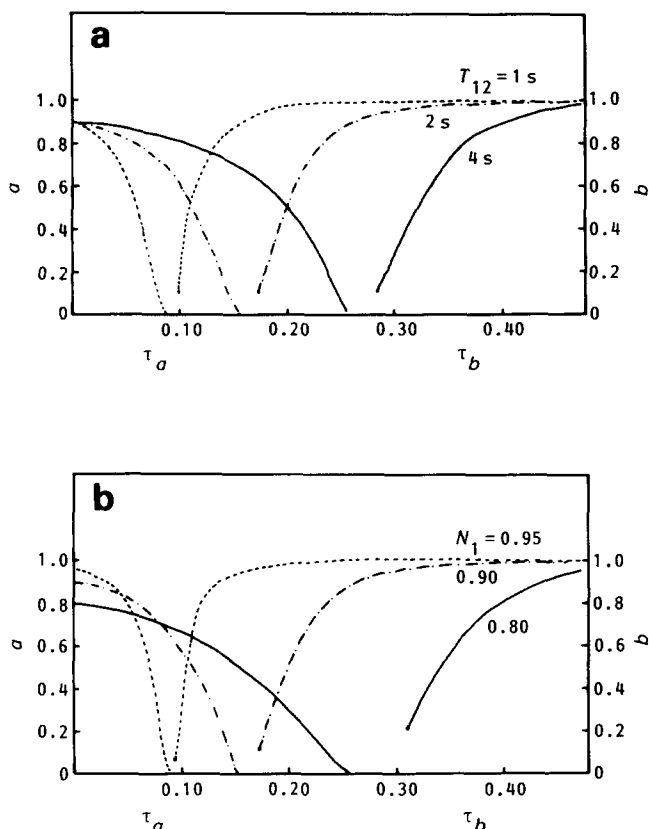


Figure 6 Relationships between τ_a, τ_b, a, b as defined by equation (10). $T_{1\rho}(1)$ is varied and $T_{1\rho}(2)$ held fixed at 0.8 s. (a) The effect of varying the cross-relaxation rate T_{12}^{-1} given $N_1 = 0.90$. (b) Influence of the relative subsystem heat capacities N_1 and $N_2 (= 1 - N_2)$ given $T_{12} = 2$ s

The a/b ratios and τ_b values for the lowest f_1 experiments can be used to fit the model parameters N_1/N_2 and T_{12} . For subsequent higher values of f_1 , the heat capacity ratio is held fixed while the cross-relaxation rate is adjusted as required to best represent the data. The highest molar mass polyethylene exhibits the slowest cross-relaxation from the tight tube to isotropic spin subsystems consistent with the smallest isotropic component amplitude, N_2 . A gradual progression to slower cross-relaxation is apparent as the r.f. field is increased. For all these experiments the calculated $T_{1\rho}(1)$ values for the dominant tight tube subsystem are close to the raw τ_a data.

Spectral density, $J_0(2\omega_1)$

In order to reveal the r.f. field dependence of the spectral density function, $J_0(2\omega_1)$ the tight tube subsystem data are plotted in Figure 7 as $\log(T_{1\rho}(1)^{-1} - 0.7T_1^{-1})$ vs. $\log(f_1)$. It should be noted that the correction for the $J_1(2\omega_1)$ and $J_2(2\omega_1)$ spectral density terms is small, as is the correction which allows for cross-relaxation effects. The spectral density functions show several remarkable features.

First, the 120 000 fraction melt exhibits a single regime from 5×10^2 to 10^5 Hz with a power law dependence $J_0(2\omega_1) \sim \omega_1^{-0.62}$. The exponent is sufficiently close to $-1/2$ to strongly suggest the motional regime $1/\tau_R^* \ll 2\omega_1 \ll 1/\tau_I$ in the Kimmich model.

Second, the data for the three molar masses exhibiting tight tube entanglement follow a common behaviour above $f_1 = 40$ kHz, an effect apparent in the data of Koch

et al.³². However in contrast with these latter experiments the $T_{1\rho}(1)$ data extend to sufficiently low frequencies that a new motional regime is established in which $M > M_c$ melt relaxation times diverge, at approximately 40 kHz for 14 000 and at 4 kHz for 32 000. Such crossovers should occur when $2\omega_1$ is comparable with τ_R^{-1} and the ratios observed here are sufficiently close to the M^3 law to be corroborative.

Third, the rate of crossover is noticeably more gentle in the more polydisperse 14 000 ($M_w/M_n = 1.27$) polyethylene than in the 32 000 ($M_w/M_n = 1.10$) melt. This suggests that the crossover frequency is strongly molar mass dependent, consistent with it being governed by tube disengagement processes.

To test this interpretation of the data the exact spectral density has been calculated using equation (12) of reference 16. For simplicity, tube disengagement is assumed to occur by reptation alone. Some justification for the neglect of contour length fluctuation is given by the low value of M_c for polyethylene. Based on a model relating mean fold lengths to zero shear viscosity¹⁶, the value of $M_c = 3800$ suggests that $\Delta_0/L_0 \leq 0.1$ for $M \geq 14000$.

Figure 8a shows the calculated $T_{1\rho}$ dispersions assuming $\tau_I = \kappa_I M$ and $\tau_R^* = \kappa_R M^3$ with numerical prefactors chosen from reference 32. Several features of the data are well represented. In particular the power law

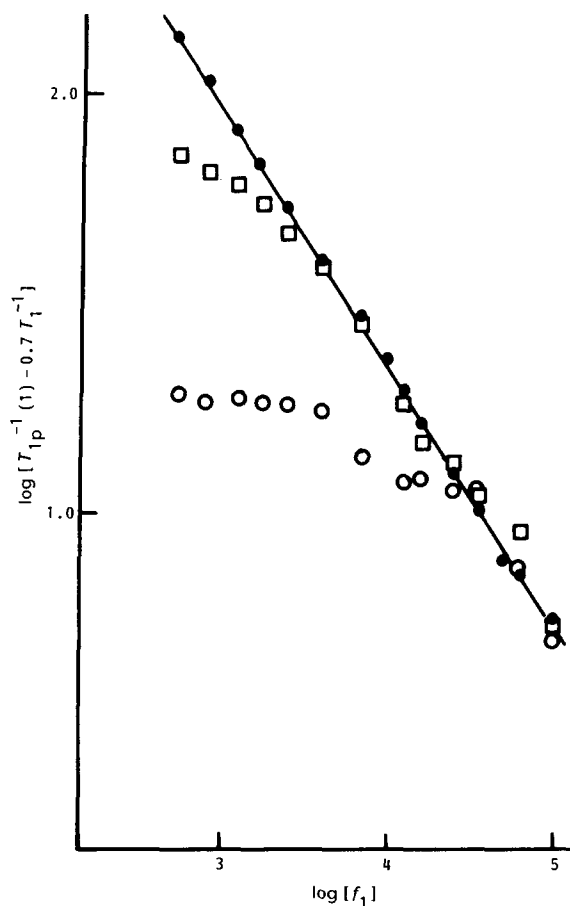
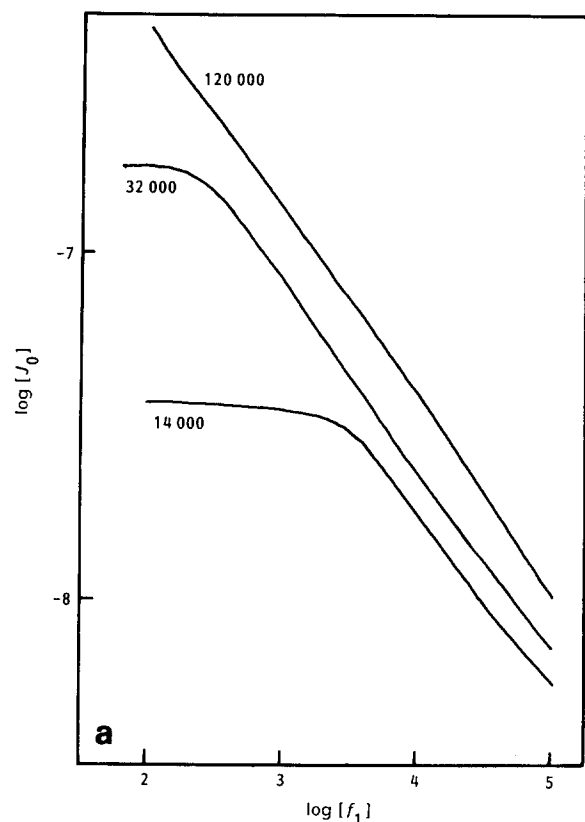


Figure 7 Rotating frame relaxation dispersions $\log(T_{1\rho}(1)^{-1} - 0.7T_1^{-1})$ vs. $\log(f_1)$ for the three polyethylene fractions with $M > M_c$. The break to the low frequency plateau apparent for the 14 000 and 32 000 melts is consistent with the crossover at $\tau_R^*^{-1}$. The intermediate frequency regime shows a common behaviour for all fractions, suggesting $\tau_I \sim M^0$. —, $f_1^{-0.62}$; ●, 120 000 fraction; □, 32 000 fraction; ○, 14 000 fraction



dependence in the intermediate frequency regime is comparable and the $\omega_1 \sim \tau_R^i$ crossovers for 14 000 and 32 000 fractions occur at the appropriate ratios albeit with different absolute values. The most significant discrepancy is with respect to the common relaxation behaviour for data in the (asymptotic) intermediate frequency regime for which the calculated dispersion shows differing relaxation rates arising from differing semi-local correlation times, τ_i . Such an identity is apparent in the 9600 and 100 000 polyethylene T_1 data of Koch *et al.* down to their lowest frequency of 30 kHz, inconsistent with their choice of $\tau_i \sim M$.

The parameters of reference 32 are now modified to provide the best fit to the present data. The κ_R^i prefactor is reduced which has the effect of shifting the fit along the $\log(f_1)$ axis. In order to represent the asymptotic coincidence of the data and to slightly increase the scaling exponent in the intermediate frequency regime a common τ_i value is chosen, slightly longer than that used for the 120 000 curve in Figure 8a. Polydispersity effects are incorporated by calculating the averaged spectral density directly using a log-normal molar mass distribution of width determined by the known M_w/M_n ratios, namely

$$P(\ln/(M)) = (\pi\sigma^2)^{-1/2} \exp(-\ln^2(M/M_0)/\sigma^2)$$

where $M_0 = (M_w M_n)^{1/2}$

and $M_w/M_n = \exp(-\sigma^2/2)$ (11)

The resulting curves shown superposed on the data in Figure 8b give a substantially improved fit. In particular the positions of crossover and relative polydispersity differences in the 14 000 and 32 000 data are well represented. The resulting semi-local and tube disengagement time constants are

$$\begin{aligned} \tau_i &= 1.1 \times 10^{-7} M^0 \text{ s} \\ \tau_R^i &= 1.0 \times 10^{-18} M^3 \text{ s} \end{aligned} \quad (12)$$

Finally, it could be argued that spin-lock conditions apply only marginally below 10^3 Hz for the 120 000 polymer. It is apparent from Figure 8b that the conclusions reached above would not be affected if this data were disregarded.

CONCLUSIONS

The $T_{1\rho}$ dispersion measurements reported here have revealed spectral features not apparent at the higher frequencies employed in earlier field cycling T_1 experiments. The crossover from intermediate to low frequency behaviour has not been previously observed clearly in relaxation dispersions for polymer melts with $M > M_c$. The rotating frame relaxation method extends the frequency range down to a regime where tube disengagement effects can be clearly observed, so providing a direct measure of τ_R on a microscopic scale, in contrast to macroscopic rheological determination via the low frequency viscoelastic relaxation.

The 'three-step motional narrowing' spectral density function derived by Kimmich gives a good description of these spectral features, especially where polydispersity effects are incorporated. However it is a remarkable feature of the present study that the intermediate

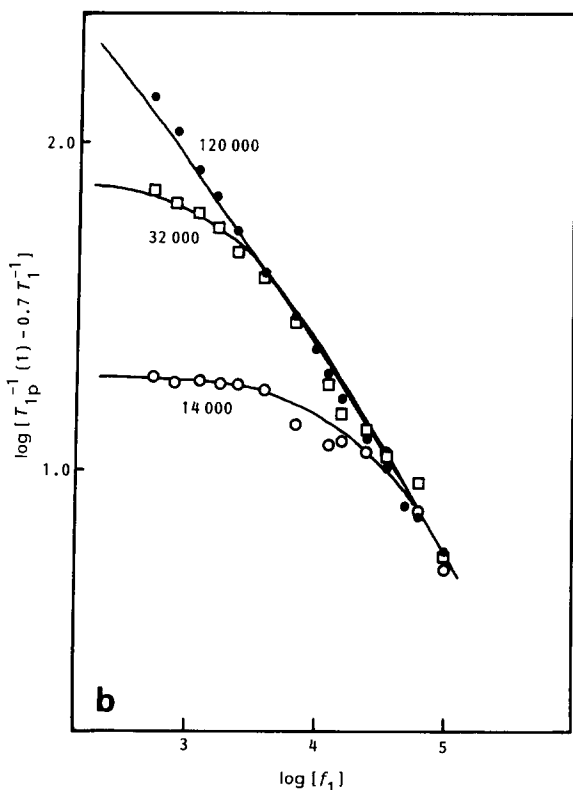


Figure 8 Theoretical $J_0(2\omega_1)$ dispersions calculated using the Kimmich tight tube model. (a) The theoretical dispersions are calculated assuming monodisperse fractions with τ_s , τ_i and τ_R^i as given in reference 32. $\tau_s = 1.5 \times 10^{-9}$ s; $\tau_i = 5.3 \times 10^{-13}$ M s; $\tau_R^i = 8.0 \times 10^{-18}$ M³ s. (b) The model is adjusted to provide a best fit to the experimental data. In particular polydispersity effects are incorporated, τ_R^i is reduced and τ_i made molar mass independent. $\tau_i = 1.1 \times 10^{-7}$ M⁰ s; $\tau_R^i = 1.0 \times 10^{-18}$ M³ s

frequency spectral density for entangled polymer does not depend on molar mass. In this respect the data presented here is consistent with earlier polyethylene T_1 measurements. A τ_1 molar mass dependence much weaker than M^1 has also been observed in T_1 measurements on polystyrene melts¹⁶.

This chain length independence suggests that the correlation loss which occurs due to curvilinear diffusion around tube bends is governed by a one-dimensional diffusion process not influenced by the total chain friction. This could be explained by considering the role of the stored length associated with chain folds. On a distance scale smaller than the mean fold separation, the one-dimensional Brownian motion need not involve the total chain but only the interfold section. Movement of this section can alter the stored length without displacing the chain centre of mass. On a larger distance scale a slower, averaged curvilinear diffusion will result from cooperative movement of the semi-local elements in which the total chain friction limits the diffusion rate and the $\tau_R \sim M^3$ law prevails.

A feature of the present study is the observation of an isotropic spin subsystem weakly coupled to the dominant tight tube spin reservoir. It is unlikely that such isotropic motion arises from low molar mass contaminants associated with polydispersity. For example the 120 000 melt exhibits an isotropic fraction of about 6%. The fraction of a $M_w/M_n = 1.20$ polymer with a molar mass below M_c is not only vanishingly small but such molecules would also be surrounded by a matrix of entangled chains. In fact the amplitudes of the isotropic fractions show a molar mass progression for the polymers with $M > M_c$ which suggests that around 5000 (or roughly twice M_c) per chain are not subject to tight tube conditions. It is tempting to identify this fraction with the chain ends.

ACKNOWLEDGEMENT

The author is grateful to P. J. Daivis for valuable discussions and for making available his non-linear least

squares fitting program, and to M. Huirua and C. D. Eccles for assistance in developing the $T_{1\rho}$ probe and associated software.

REFERENCES

- 1 Edwards, S. F. *Proc. Phys. Soc.* 1967, **92**, 9
- 2 Edwards, S. F. *Polymer* 1985, **26**, 163
- 3 Doi, M. and Edwards, S. F. 'The Theory of Polymer Dynamics', Oxford, 1986, p. 188
- 4 de Gennes, P. G. 'Scaling Concepts in Polymer Physics', Cornell University Press, Ithaca, 1979, p. 34
- 5 Ferry, J. D. 'Viscoelastic Properties of Polymers', 3rd Edn., Wiley, New York, 1980, p. 241
- 6 de Gennes, P. G. *J. Chem. Phys.* 1971, **55**, 572
- 7 Graessley, W. W. *Adv. Polym. Sci.* 1982, **47**, 67
- 8 Green, P. F. and Kramer, E. J. *Macromolecules* 1986, **19**, 1108
- 9 Doi, M. and Edwards, S. F. *J. Chem. Soc. Faraday Trans.* 1978, **74**, 1789
- 10 Nicholson, L. K. *Contemp. Phys.* 1981, **2**, 451
- 11 Callaghan, P. T. *Aust. J. Phys.* 1984, **37**, 359
- 12 Kimmich, R. *Polymer* 1975, **16**, 851
- 13 Kimmich, R. *Colloid Polym. Sci.* 1976, **254**, 918
- 14 Kimmich, R. *Polym. Prepr.* 1981, **22**(1), 109
- 15 Kimmich, R. *Polymer* 1977, **18**, 233
- 16 Kimmich, R. *Polymer* 1984, **25**, 187
- 17 Voigt, G. and Kimmich, R. *Polymer* 1980, **21**, 1001
- 18 Look, D. C. and Lowe, I. J. *J. Chem. Phys.* 1966, **44**, 2995
- 19 Roeder, S. B. W. and Douglass, D. C. *J. Chem. Phys.* 1970, **52**, 5525
- 20 Redfield, A. G. *Phys. Rev.* 1955, **98**, 1787
- 21 Abragam, A. 'The Principles of Nuclear Magnetism', Oxford University Press, Oxford, 1961, p. 264
- 22 Bloembergen, N., Purcell, E. M. and Pound, R. V. *Phys. Rev.* 1948, **73**, 679
- 23 Cohen-Addad, J. P. *J. Chem. Phys.* 1976, **64**, 3438
- 24 Cohen-Addad, J. P. *Macromolecules* 1985, **18**, 1101
- 25 Cohen-Addad, J. P. *Polymer* 1985, **26**, 97
- 26 Anderson, P. W. and Weiss, P. R. *Rev. Mod. Phys.* 1953, **25**, 269
- 27 Powles, J. G., Hartland, A. and Kail, J. A. E. *J. Polym. Sci.* 1961, **55**, 361
- 28 Cohen-Addad, J. P., Domard, M. and Boileau, S. *J. Chem. Phys.* 1981, **75**, 4107
- 29 Schumacher, R. T. *Phys. Rev.* 1958, **112**, 837
- 30 Eccles, C. D. and Callaghan, P. T. *JEOL News* 1987, **23A**, 10
- 31 Meiboom, S. and Gill, D. *Rev. Sci. Instr.* 1959, **29**, 688
- 32 Koch, H., Bachus, R. and Kimmich, R. *Polymer* 1980, **21**, 1009